C: Surfaces, Interfaces, Porous Materials, and Catalysis

Initial Steps of Oxidative Etching of MoS Basal Plane Induced by O

Lucas M. Farigliano, Patricia A. Paredes-Olivera, and Eduardo Martin Patrito

J. Phys. Chem. C, **Just Accepted Manuscript** • DOI: 10.1021/acs.jpcc.0c02141 • Publication Date (Web): 22 May 2020

Initial Steps of Oxidative Etching of MoS_2 Basal Plane Induced by O_2

Lucas M. Farigliano[a], Patricia A. Paredes-Olivera[b], Eduardo M. Patrito[a*]

[a]Departamento de Fisicoquímica and [b]Departamento de Química Teórica y Computacional. Instituto de Investigaciones en Físico Química de Córdoba (INFIQC). Facultad de Ciencias Químicas, Universidad Nacional de Córdoba, X5000HUA Córdoba, Argentina.

Abstract

We have investigated the first stages of oxidation of the basal plane of MoS_2 with O_2. The different intermediates in the energy landscape were found at 0 K with nudged-elastic band calculations and their reactivity was evaluated at higher temperatures by performing ab-initio molecular dynamics simulations. We identified the intermediates and mechanisms leading to the desorption of both SO and SO_2 species. The key intermediate consists of an O atom bound on top of an S atom with a second O atom inserted into the S−Mo bond, giving rise to a stable O=S−O−Mo moiety. The mechanisms leading to this intermediate upon adsorption of O_2 on the basal plane of MoS_2 are discussed. From the O=S−O−Mo intermediate, SO_2 may desorb directly generating a single sulfur vacancy on the surface while its decomposition leads to the desorption of SO and leaves substitutional oxygen on the surface. These etching mechanisms were also observed in the ab-initio molecular dynamics simulations in good agreement with energy profiles calculated along the reaction paths. Diffusion of O atoms on top of the sulfur layer and direct desorption of SO groups were never observed in the molecular dynamics simulations because these processes have high energy barriers (2.4 eV and 3.1 eV, respectively). However, subsurface diffusion of O atoms, involving the formation of both O−S and O–Mo bonds, is a competing process with lower energy barriers.

1. Introduction

Two-dimensional (2D) molybdenum disulfide has received great attention as a potential material for fabricating ultrathin electronic devices owing to its semiconductor bandgap.[1] The applications of MoS_2 in electronic and optoelectronic devices require the material to be chemically stable. Understanding its stability in ambient conditions is crucial for the development of potential applications. The performance of MoS_2 based Field-Effect Transistors, for example, can be significantly affected by environmental gases such as oxygen and water.[2] CVD-grown sheets develop extensive cracking and show a severe quenching of the direct gap photoluminescence after exposure to the environment for several months.[3] The oxidation induced etching observed originates from edges and grain boundaries and proceeds towards the interior of the flakes.[3] The oxidation of thin MoS_2 flakes begins along the flake boundary, forming beads of decomposed material along its edges which has been attributed to the desorption of sulfur dioxide and formation of MoO_3.[4]

Monolayers and multilayers rapidly oxidize upon exposure to elevated temperatures in an ambient atmosphere. Oxidative etching starts at defects on the basal planes and the edges.[5] MoS_2 edges tend to oxidize faster than the basal plane due to the lower coordination of the edge Mo atoms. Oxidative attack on the basal planes leads to the formation of triangular microscopic etch pits.[6,7] Exfoliated MoS_2 is shown to chemically oxidize in a layered manner upon exposure to a remote O_2 plasma.[8] Multilayer films can be thinned down to 1 or 2 layer patches at high temperatures in the presence of O_2.[9] The oxidation of MoS_2 usually produces areas covered by MoO_3 that can subsequently volatilize and lead to etching.[10]

The mechanisms of MoS_2 oxidative etching are not yet fully understood. Many processes are involved depending on the temperature and the environmental conditions. The surface diffusion of initially physisorbed oxygen has been pointed out as an important step in the MoS_2 oxidation mechanism.[11] S atoms on the basal plane of MoS_2 can also exchange with O atoms upon exposure to the atmosphere either

at room temperature[12] or elevated temperatures.[13] However, at around 280 ºC the oxidation mechanism changes from oxygen substitution to full MoO_3 conversion.[13] The basal plane oxygen exchange can be performed selectively without edge oxidation when the edges are fully sulfided.[13] In the absence of O_2, defective MoS_2 can be formed under heat treatment by desorption of MoS_x species.[14] In the case of thick geological MoS_2 crystals exposed to air, the heat-induced oxidative etching kinetics was characterized by the growth of triangular etch pits. It was concluded that the series of etching events taking place mainly proceed along zig-zag Mo edges.[15] Monolayers and bilayers of MoS_2 which were previously irradiated with low doses of He^+ can be etched with high region specificity after heating in air.[16] The selective functionalization of the basal plane of MoS_2 with oxygen atoms allows tuning both the electronic properties and chemical reactivity of MoS_2. Although the edges of the single-layer MoS_2 are known to be highly active for catalysis,[17] now there is also interest in activation of the basal plane by substitutional oxygen to promote the hydrogen evolution reaction.[12,18,19]

Semiconductor device fabrication technology requires to easily control patterning and etching processes. The main products of MoS_2 oxidation are SO_2 and MoO_3.[20] Thus, in the oxidative etching process, the sample thins via evaporation of SO_2 molecules as well as through the production of MoO_3 oxides which can also be volatilized upon heating to the appropriate temperature. Before molybdenum oxides can be formed, SO_2 desorption must occur to allow further reactions of Mo with oxygen species.[21] In the case of edges, O_2 binds to edge sulfur atoms and the detachment of SO_2 leaves a sulfur vacancy into which oxygen atoms can bind to finally yield MoO_3.[21] SO_2 desorption from the basal plane has been proposed to occur via an oxygen-induced single sulfur vacancy creation mechanism.[12] Other oxidation mechanisms might also occur, for example, in a study of hyperthermal atomic oxygen interaction with MoS_2, the main desorption product is SO rather than SO_2.[22]

The reactivity of MoS_2 towards O_2 was investigated using DFT calculations. Two works inform an energy barrier of 1.59 eV[23,24] for the dissociative adsorption of the oxygen molecule on the basal plane of MoS_2 whereas another work informs a smaller value of 1.1 eV.[12] When the same process occurs on an S-defective site, the energy barrier is halved.[23] The edge sites are still more reactive with an O_2 dissociation barrier as low as 0.31 eV.[21]

Previous theoretical investigations have only considered the initial steps in the reaction of O_2 with the basal plane of MoS_2 and these quantum mechanical calculations explored the potential energy hypersurface only at a temperature of 0 K.[12,23,24] The detailed mechanistic steps and the molecular dynamics processes leading to the formation of sulfur oxides during the oxidative etching of the basal plane of MoS_2 by O_2 have not been investigated yet in detail. In this work, we identified the intermediates and the reaction mechanisms that lead to the desorption of SO and SO_2 molecules. We first present the results of nudged elastic-band calculations which allowed us to characterize the potential energy surface along reaction paths at 0 K. We found that five intermediates are involved in the different elementary reaction steps. For each of them, we next performed extensive Ab-initio molecular dynamics simulations in order to follow decomposition mechanisms at higher temperatures. In this way, we present a complete picture of the oxidation of the basal plane of MoS_2 by O_2 in the absence of surface defects. The same reaction mechanisms were found at 0 K and high temperatures, indicating that the potential energy surface is not appreciably affected by temperature, as expected from the high mechanical stability of MoS_2.

2. Theoretical Methods and Surface Modelling

Density-functional theory (DFT) calculations were performed with the Perdew–Burke–Ernzerhof (PBE) exchange-correlation functional[25] and norm-conserving ultrasoft pseudopotentials[26] as implemented in the Quantum Espresso (QE) package.[27] The electron wave functions were expanded in a plane-wave basis set up to a kinetic energy cutoff of 40 Ry (240 Ry for the density). All calculations involving the adsorption

of O_2 were performed with spin polarization. Several test calculations performed with spin polarization showed that once S−O and/or Mo−O bonds were formed, the cell had no net spin and therefore, spin polarization was not included in order to speed up the costly molecular dynamics calculations. Dispersive forces were introduced using Grimme's semiempirical DFT-D2 approach[28] as implemented in the PWscf code[29] of QE. Reaction pathways were calculated with the climbing-image nudged-elastic-band (CI-NEB) method as implemented in QE.[30]

The CI-NEB calculations were performed using a (3×3) MoS_2 superstructure and the integration in the first Brillouin zone was performed with a (4×4×1) Monkhorst−Pack mesh.[31] In some test calculations, larger unit cells were employed as indicated in the text. For the ab initio molecular dynamics simulations (AIMD) we employed a 3√3×6 supercell with dimensions 16.71 Å × 19.30 Å. For this large cell, only one k point (gamma) was used for integration to obtain a good balance between the number of atoms used and the computational burden. All supercell dimensions were optimized using the "vc-relax" option of QE. A time step of 1 fs was used in the MD simulations and the temperature was controlled using a Berendsen thermostat at 100 K, 300 K, and 1500 K. The high temperature of 1500 K was used to speed up the MD simulations. The longest simulations were performed up to around 12 picoseconds, implying 12,000 simulation steps.

3. Results and Discussion

The goal of this paper is to find the mechanisms that lead to the etching of the basal plane of MoS_2 via the release of either SO or SO_2 towards the gas phase. Consequently, we performed an extensive search of intermediates involved in these mechanisms. For that purpose, we used a combined approach employing both the NEB method and AIMD simulations at different temperatures. The NEB approach may suffer from the drawback that some chemical intuition is needed about possible mechanisms when defining the initial and final states. If the defined process does not correspond to an elementary reaction step,

intermediates (local minima in the potential energy surface) may be found in between and finally one must prove that a given energy path effectively connects two intermediates. To overcome these difficulties, we performed AIMD simulations with the first set of intermediates found from NEB calculations which allowed us to find new intermediates as well as to verify elementary reaction steps. In this way, we could identify a set of intermediates consistent with both NEB and AIMD calculations.

3.1 Minimum Energy Pathways from NEB calculations. Figure 1 shows side and top views of the structure of reactants (Figure 1a), products (Figure 1b) and intermediates (Figure 1c). Using the combined NEB + AIMD strategy, we found five intermediates (Figure 1c). Below each panel, we show the nomenclature used to identify each structure and the relative energy taking as the reference state the energy of the reactants (Figure 1a, an O_2 molecule physisorbed ontop of a sulfur atom of the MoS_2 layer). Figure 1b shows the SO_2 (panel I) and SO (panel II) products adsorbed on the surface. Desorption of SO_2 leaves a sulfur vacancy on the surface (Figure 1b, panel I) whereas desorption of SO leaves an O-doped surface in which an S atom of MoS_2 is replaced by an O atom (Figure 1b, panel II).

In the O_2-S intermediate (Figure 1c, panel I) a distorted O_2 molecule is chemisorbed on an S atom. The long O-O distance of 1.55 Å indicates that a single bond exists between the O atoms (the bond length is 1.24 Å in the gas phase). The SO+SO intermediate (Figure 1c, panel II) corresponds to two O atoms bound on top of adjacent S atoms. In the OSOMo intermediate (Figure 1c, panel III) there is an O atom inserted into an S−Mo bond and a second O atom is bound to this S atom. The Mo−OSO intermediate (Figure 1c, panel IV) corresponds to an SO_2 molecule with one of the O atoms bound to two adjacent Mo atoms whereas the S atom is above the plane of the remaining S atoms of the surface. In the SO+SOMo intermediate (Figure 1c, panel V) there is an O atom inserted into an S-Mo bond whereas the other O atom is bound on top of an adjacent sulfur atom. None of the intermediates in Figure 1c have a net spin density (no net spin was observed in the unit cell).

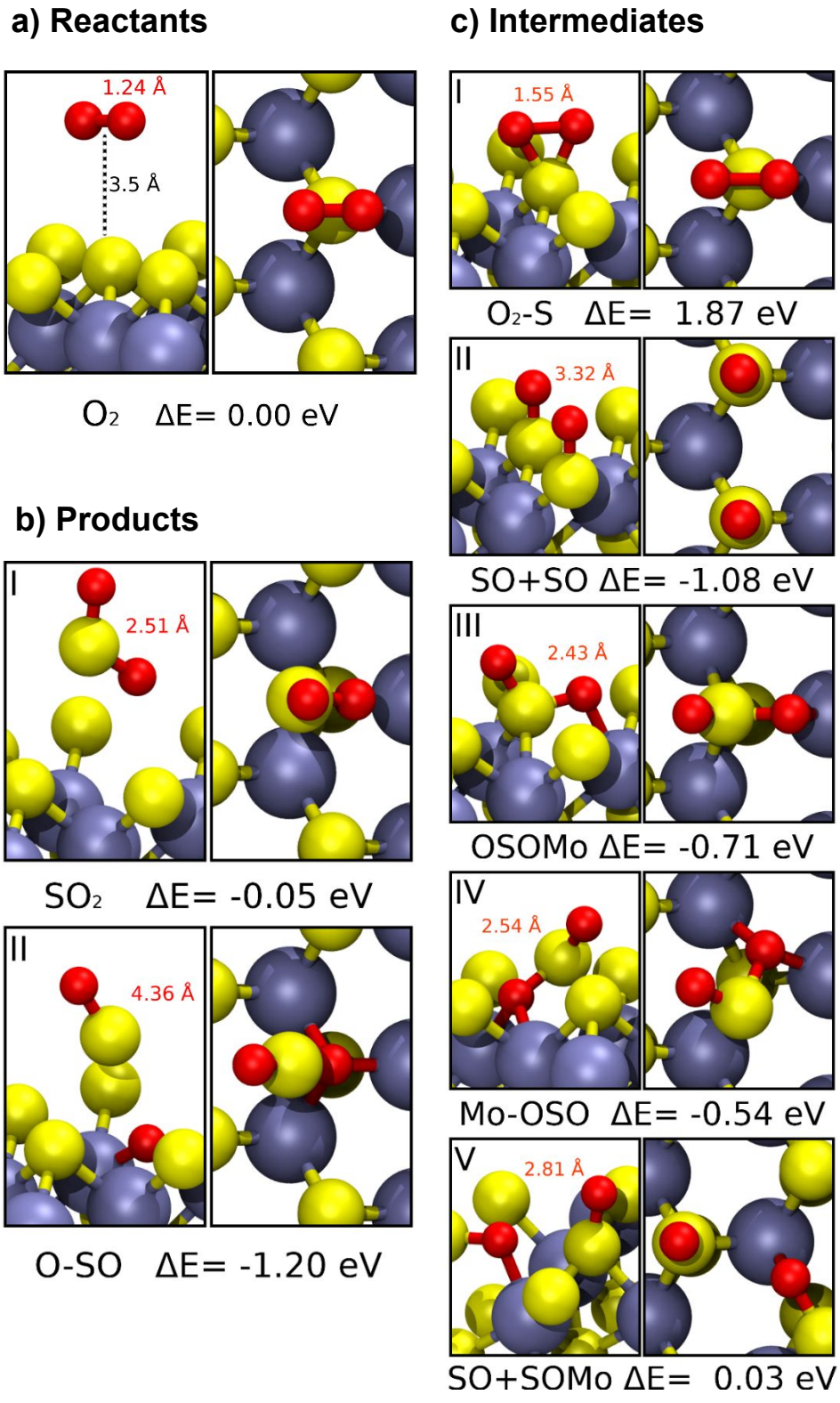

Figure 1. Side and top views of the structure of **a)** reactants, **b)** products and **c)** intermediates found in the reaction of O_2 with the basal plane of MoS_2. The ΔE values are calculated taking as reference the energy of the reactants. The labels below each panel show the nomenclature used to identify every structure.

The ΔE values for the products (Figure 1b) show that the release of SO is much more exothermic than the release of SO_2 (-1.20 eV vs -0.05 eV, respectively). This is because an S atom of the surface is substituted by an O atom in the first case, whereas a reactive sulfur vacancy is left on the surface upon desorption of SO_2. The calculations of Santosh et al. have shown that the substitution of sulfur by oxygen atoms is a thermodynamically competitive process in a wide range of oxygen pressures.[23]

The most stable intermediate is the SO+SO (Figure 1c, panel II) with ΔE=-1.08 eV, followed by the OSOMo (panel III) and Mo−OSO (panel IV) intermediates, with ΔE values of -0.71 eV and -0.54 eV, respectively. The O_2-S intermediate lies 1.87 eV above the energy of the reactants (panel I) whereas the SO+SOMo intermediate (panel V) has ΔE=0.03eV. The intermediates in Figure 1c are true local minima in the potential energy surface. Their stability was checked by performing AIMD simulations during 1 ps at 100 K. Figure S1 shows that the total energy profile remains constant during this time window which allows for several S-O vibrations. The relative energy of intermediates shown in the profiles in Figure S1 at 100 K has the same trend as that shown in Figure 1c, corresponding to a 0 K temperature.

Figure 2 shows the energy profiles along the reaction path connecting the different intermediates. The numbers in the figure correspond to the energy barriers relative to the previous energy minimum. The reaction of O_2 with the MoS_2 surface may initiate with either the O_2-S intermediate (Figure 1c, panel I) or the SO+SO intermediate (Figure 1c, panel II) and after the initial steps, both reaction branches converge to the OSOMo intermediate (Figure 1c, panel III). The energy profile of the series of reactions that proceed via the SO+SO intermediate is shown in Figure 2a, whereas Figure 2b shows the energy profile of the reactions that proceed via the O_2-S intermediate. The energy pathway of the final reaction steps that initiate with the OSOMo intermediate and end with the release of either SO_2 or SO species is shown in Figure 2c.

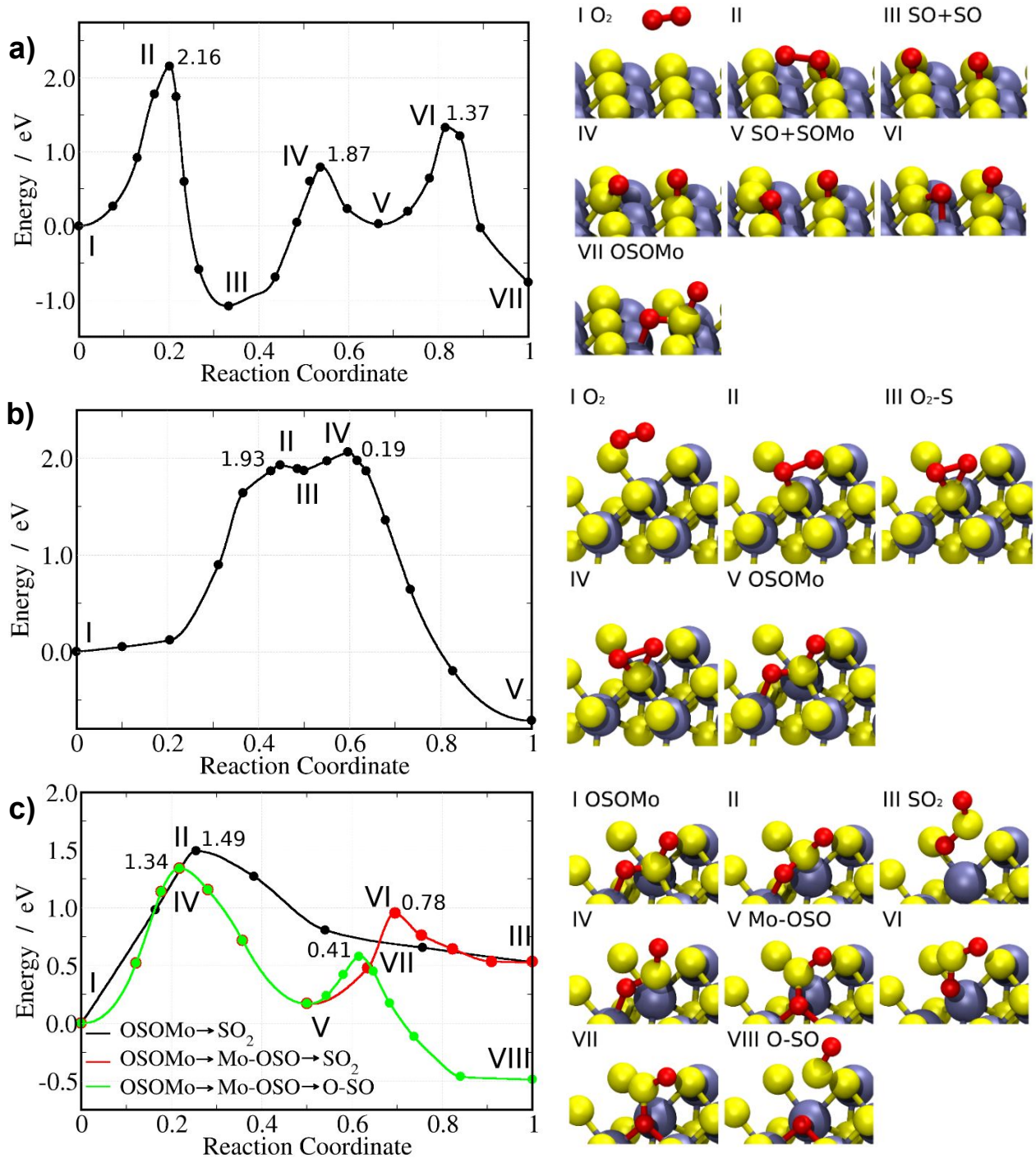

Figure 2. Energy profiles obtained from NEB calculations connecting reactants, intermediates, and products. The numbers correspond to activation energy values (in eV) calculated with respect to the previous local minimum. The panels on the right show the structure of representative points along the energy path. **a)** Reaction path proceeding along the SO+SO intermediate (panel III) and ending in the OSOMo intermediate (panel VII). **b)** Reaction path along the O_2-S intermediate (panel III) ending in OSOMo intermediate (panel V). **c)** Energy profiles starting from OSOMo intermediate leading to the desorption of SO_2 (panel III) or SO (panel VIII).

Figure 2a shows that the dissociative adsorption of O_2 (panel I) yielding two adjacent SO groups (panel III) is exothermic with ΔE=-1.08 eV and has a high energy barrier of 2.16 eV. The next intermediate is obtained when one O atom of SO inserts into the S−Mo bond yielding the SO+SOMo intermediate (panel V of Figure 2a) after surpassing a barrier of 1.87 eV. Next the O atom in the SOMo moiety inserts into the Mo–S bond of the adjacent SO group yielding the OSOMo intermediate (Figure 2a, panel VII). This process has a barrier of 1.37 eV. The OSOMo intermediate has been reported in previous work.[12] However, the NEB calculations in ref. (12) failed to identify that the conversion from the SO+SO intermediate (Figure 2a, panel III) to the OSOMo intermediate (Figure 2a, panel VII) is not an elementary reaction step as the SO+SOMo intermediate is first observed (Figure 2a, panel V).

The OSOMo intermediate can be reached straightforwardly via the pathway shown in Figure 2b. After the formation of the O_2-S intermediate (Figure 2b, panel III) with an energy barrier of 1.93 eV, one of the O atoms inserts into the S–Mo bond, and the stable OSOMo intermediate is formed (Figure 2b, panel V) with ΔE = -0.71 eV. From the OSOMo intermediate, several reaction pathways are possible, as shown in Figure 2c. The direct desorption of SO_2 leaving a vacancy on the surface has a high barrier of 1.49 eV. The breakage of S–Mo bonds of the S atom in the OSOMo intermediate yields the Mo−OSO intermediate (Panel V). The barrier to reaching this intermediate is 1.34 eV. Finally, from this intermediate two competing pathways are observed. In the first one, the SO_2 molecule may desorb after breakage of Mo–O bonds with a barrier of 0.78 eV, leaving a sulfur vacancy on the surface (Panel III). In the second one, one O–S bond breaks leaving an adsorbed O atom and a desorbed SO molecule (Panel VIII). Desorption of SO has been reported experimentally as the main product in a study of hyperthermal atomic oxygen with MoS_2 surfaces.[22]

The ΔE value of -1.08 eV that we obtained for the dissociative adsorption of O_2 yielding two SO moieties (Figure 2a) agrees with the values close to -1 eV reported in previous works.[12,14] However, there is a large

discrepancy regarding the energy barrier informed in these works, with values of 1.1 eV[12] and 1.6 eV[24], with our value of 2.16 eV. It is known that the type of functional employed in DFT calculations may influence barrier heights.[32] However, in this work as well as in refs. (12) and (24), the same PBE functional[25] was used. Both in refs. (12) and (24) as well as in this work, the Climbing Image NEB method[30] has been used to obtain the energy profile along the reaction path. Notably, the same computational program (VASP) was used in the previous works[12,24] however, the informed energy barriers differ by 0.5 eV. We think that the discrepancies arise from the poor exploration of the total energy hypersurface during the search of the reaction path when using the CI-NEB method.[30] Henkelman et at. outline that the shape of the energy profile along the reaction coordinate is often highly asymmetric in dissociative adsorption processes.[30] Therefore they suggest using stronger spring constants connecting adjacent images near the saddle point and weaker ones for images with low energies. This produces an uneven distribution with more images closer to the saddle point. This guarantees that the climbing image will effectively converge to a saddle point.[30] In Fig. S2a we show energy profiles calculated with 5 and 7 images using both constant and variable springs. We obtained energy barriers between 0.88 eV and 2.08 eV, with the lowest values for calculations with constant springs (which produce an even distribution of energy points along the reaction coordinate, see the profiles with open symbols in Fig. S2a). However, when 9 and 13 images are used together with variable spring constants, the energy barrier converges to the value of 2.16 eV. In ref. (12) the energy points along the reaction path are not presented and in ref. (24) only 7 images with equal spacing along the reaction coordinate were used, which indicates that constant springs were employed between the images. This does not guarantee the convergence of the climbing image to the saddle point.[30] Therefore, we conclude that the energy barriers reported in refs. (12) and (24) are underestimated.

3.2 Stability of Intermediates: Ab-initio Molecular Dynamics. The mechanisms shown in Figure 2 obtained from NEB calculations correspond to 0 K temperature. We now show that they are confirmed by AIMD simulations at higher temperatures. To get more statistical information from the simulations, we employed a large unit cell in which four intermediates of the same type could be accommodated. Figure 3a shows the evolution of the energy profile during a simulation with four O_2–S intermediates at 300 K. The insets show top and side views of the unit cell. The simulation was started with the unit cell previously equilibrated at 100 K (Figure S1). The short energy peak during the first 0.1 ps occurs during the thermostatization to the new temperature of 300 K. Each energy step in Figure 3a corresponds to the exothermic process in which an O_2–S intermediate converts into the more stable OSOMo intermediate. The red curve in the energy profile corresponds to one such process. The panels in Figure 3b are snapshots of the simulation taken at the indicated time in the inset. Figure 3b shows that once the O–O breaks, one of the O atoms inserts into the S–Mo bond whereas the other O atom remains on top of the S atom, thus yielding the stable OSOMo intermediate (panels III-VI). The simulation shows an energy jump of -2.6 eV for this process (see inset in Figure 3a) in good agreement with the value of -2.59 eV which is obtained from the NEB calculation in Figure 2b. During the 1 ps simulation, 3 out of the 4 O_2–S intermediates converted into the OSOMo intermediate. This is readily observed in the variation of the O–O bond distance shown in Figure 3c. The O atoms in the O_2–S intermediate vibrate at around 1.56 Å and this distance sharply increases when the O atoms move away to form the OSOMo intermediate (black, red, and green curves in Figure 3b). The blue curve in Figure 3b corresponds to the O_2–S intermediate that remained stable during the simulation time.

Except for the O_2–S intermediate, all the others are stable at 300 K within a few picoseconds of simulation time. Figure S3 compares the energy profiles of the five intermediates at 300 K during the first picosecond. To accelerate the simulations, the temperature was next raised to 1500 K. Figure 4a compares the energy

profiles for the OSOMo (black curve), Mo–OSO (red curve) and SO+SOMo (green curve) intermediates (see Figure 1c).

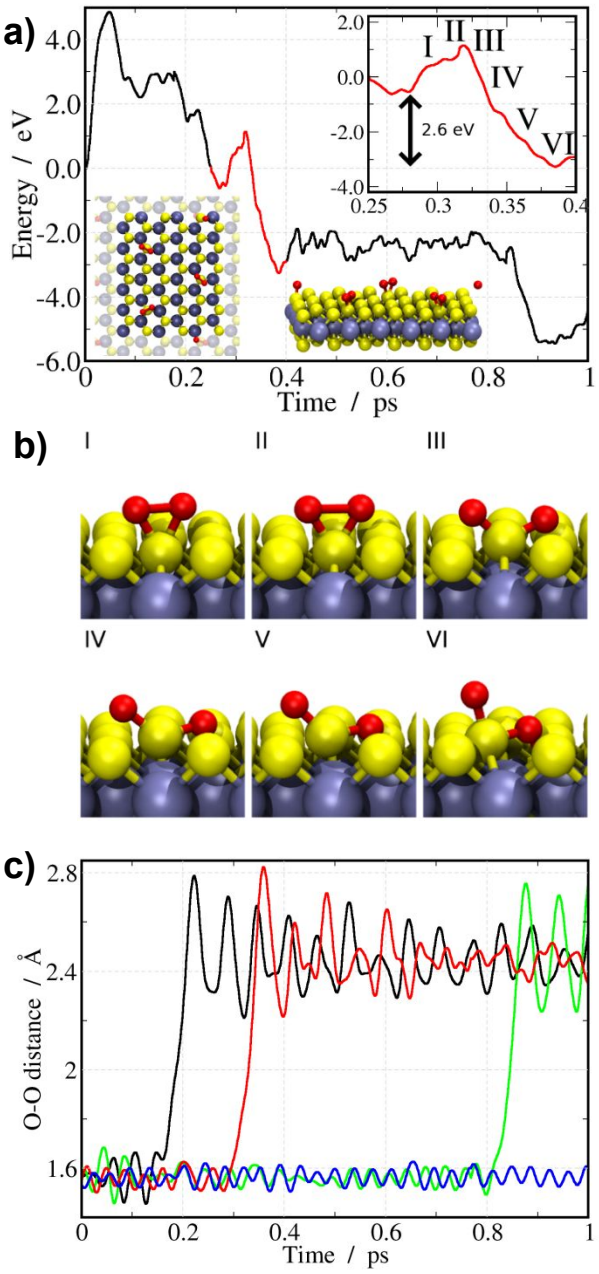

Figure 3. a) Total energy as a function of time for the AIMD simulation performed at 300 K in a MoS_2 cell initially containing four O_2-S intermediates (see inset). **b)** Snapshots along the red curve in the energy profile showing the decomposition of the O_2-S intermediate to yield the OSOMo intermediate (panel VI). **c)** O−O bond distance as a function of time for each of the four intermediates in the simulation cell. Three of them react to yield the OSOMo intermediate in which the O atoms are separated by 2.6 Å on average.

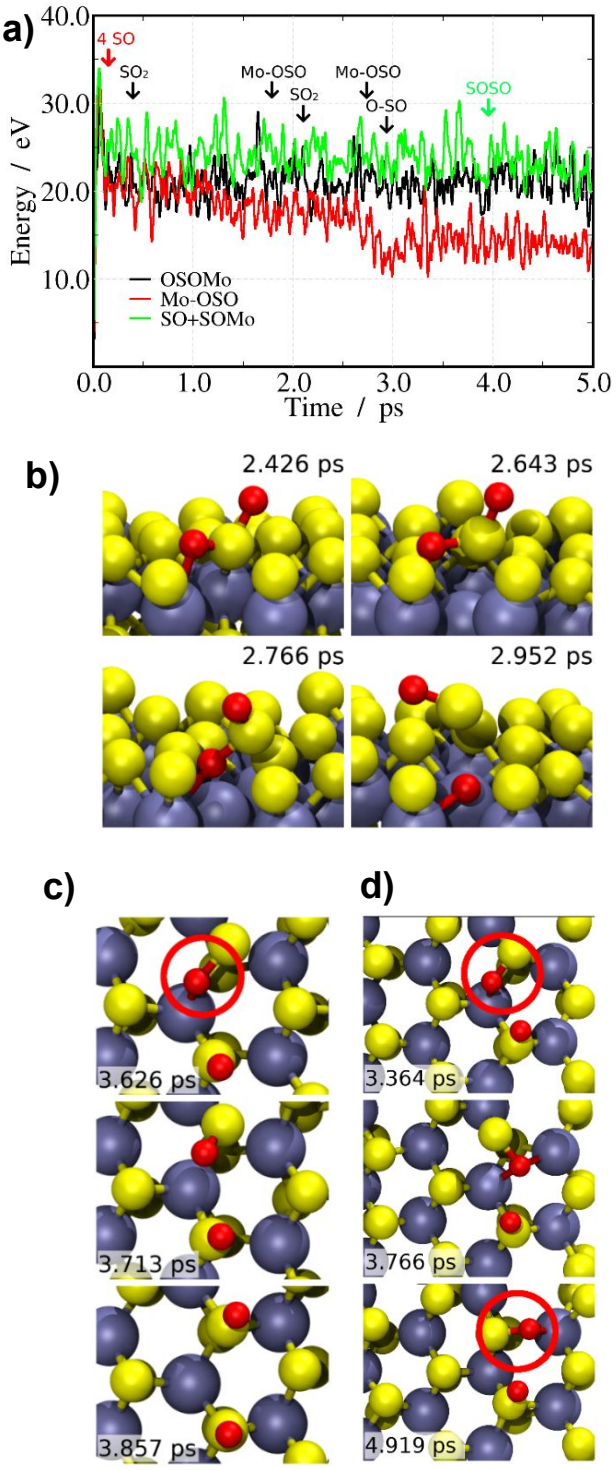

Figure 4. a) Evolution of total energy as a function of time for AIMD simulations performed at 1500 K for OSOMo (black curve), Mo−OSO (red curve) and SO+SOMo (green curve) intermediates. In all cases, there are four intermediates in the simulation box. **b)** Snapshots showing the conversion of an OSOMo intermediate into a Mo−OSO intermediate (2.766 ps) which decomposes releasing an SO molecule and leaving an O atom adsorbed on the surface (2.952 ps). **c)** Snapshots showing the conversion of a SO+SOMo intermediate into a SO+SO intermediate after the breakage of a Mo−O bond (3.626 ps, red circle). **d)** Snapshots showing the subsurface diffusion of an O atom around an S atom (red circle) after breaking a Mo−O bond and formation of a new one.

In each simulation, there are four intermediates in the unit cell. The arrows indicate the time when a specific structural rearrangement has occurred or when a species has desorbed. The large energy fluctuations at high temperatures mask, in general, the small ΔE values associated with the different reactions. In the case of the simulation with four OSOMo intermediates (Figure 4a, black curve), two of them yielded SO_2 desorption (at 0.432 ps and 2.105 ps), one of them decomposed releasing SO (at 2.910 ps) and the fourth remained stable during the 5 ps simulation time. Figure 4b illustrates the structural changes leading to the desorption of SO. The OSOMo intermediate shown at 2.426 ps converts into Mo–OSO intermediate after breakage of S–Mo bonds (2.766 ps). In the last panel at 2.952 ps the O–S bond is broken, and SO is released to the gas phase. The OSOMo to Mo–OSO conversion before the desorption of SO shown in Figure 4b agrees with the reaction pathway in Figure 2c. The simulation with four Mo−OSO intermediates (Figure 4a, red curve) readily showed the release of four SO molecules to the gas phase as indicated by the arrow at 0.1 ps. This is consistent with the small energy barrier of this process (0.41 eV, Figure 2c). The decrease in the total energy observed in Figure 4a at 2.9 ps after desorption of the four SO molecules is due to further reactions among them in the gas phase yielding SO_2 and SO species (Figure S4).

The NEB calculation in Figure 2a shows that in the forward direction, the sequence of intermediates is SO+SO → SO+SOMo → OSOMo. This sequence, however, was never observed in the AIMD simulations. The SO+SO intermediate remained stable during the whole simulation time at 1500 K. Figure S5a shows that the energy remained stable and Mo−O bonds were not formed (Figure S5b). In the simulation with four SO+SOMo intermediates (Figure 4a, green curve) we only observed the backward reaction SO+SOMo → SO+SO as illustrated by the snapshots in Figure 4c. According to the energy profile in Figure 2a, this process has a barrier of 0.76 eV. However, we did not observe the forward reaction in which the SO+SOMo intermediate converts into the OSOMo moiety, with a barrier of 1.37 eV as shown

in Figure 2a. We remark that at 1500 K the system has enough potential energy to overcome such a barrier height. For example, as discussed above, we have observed processes with higher barriers such as the desorption of SO_2 (1.49 eV barrier, Figure 2c) or the OSOMo → Mo–OSO conversion (1.34 eV barrier, Figure 2c). We, therefore, conclude that the forward reaction (SO+SOMo → OSOMo) corresponds to a path with a low probability. The snapshots in Figure 4c show that the SO+SOMo → SO+SO conversion is a straightforward process as it only involves the breakage of a Mo–O bond (panel at 3.626 ps in Figure 4c, indicated by a circle) leading to the formation of a new SO group (panel at 3.857 ps in Figure 4c). On the contrary, the forward reaction SO+SOMo → OSOMo is a complex process that requires the breakage of the S–OMo bond and the insertion of the O atom into the S–Mo bond of the adjacent SO group to finally yield the OSOMo intermediate. Finally, the snapshots in Figure 4d show a different process occurring around the SOMo moiety. It is the diffusion of an O atom to an adjacent surface site, involving the breakage and formation of Mo−O bonds. We will refer to such a process as subsurface oxygen diffusion. In summary, after the first 5.0 ps of simulation time, we observed that one of the four SO+SOMo intermediates converted into the SO+SO intermediate (Figure 4c) whereas the O atom in a SOMo moiety diffused towards and adjacent position (Figure 4d).

From the structure at 5.0 ps, the AIMD simulation was extended for another 12 picoseconds yielding the energy profile in Figure 5. At 2 and 11 ps we observed the formation of two new SO+SO intermediates. The energy profile averaged in the last picosecond of simulation is 2.55 eV lower than during the first picosecond, which is consistent with the formation of two SO+SO intermediates. From Figure 1c the energy difference for the conversion SO+SOMo → SO+SO is ΔE = -1.11 (Figure 2a), therefore yielding ΔE = - 2.22 eV for two intermediates, in agreement with the AIMD simulation. The final structure after 12 ps is shown in Figure 5b and contains 3 SO+SO intermediates and one SOMo moiety. As outlined above, the SO+SOMo → OSOMo conversion was not observed either at these long simulation times. It

is important to remark that neither in the simulations containing SO+SO intermediates nor in simulations with SO+SOMo intermediates did we observe desorption of sulfur species. We, therefore, conclude that the mechanism leading to the formation of SO groups after O_2 dissociation (Figure 2a) does not lead to desorption of SO_2, because the SO+SO intermediate produced in this mechanism is very stable and does

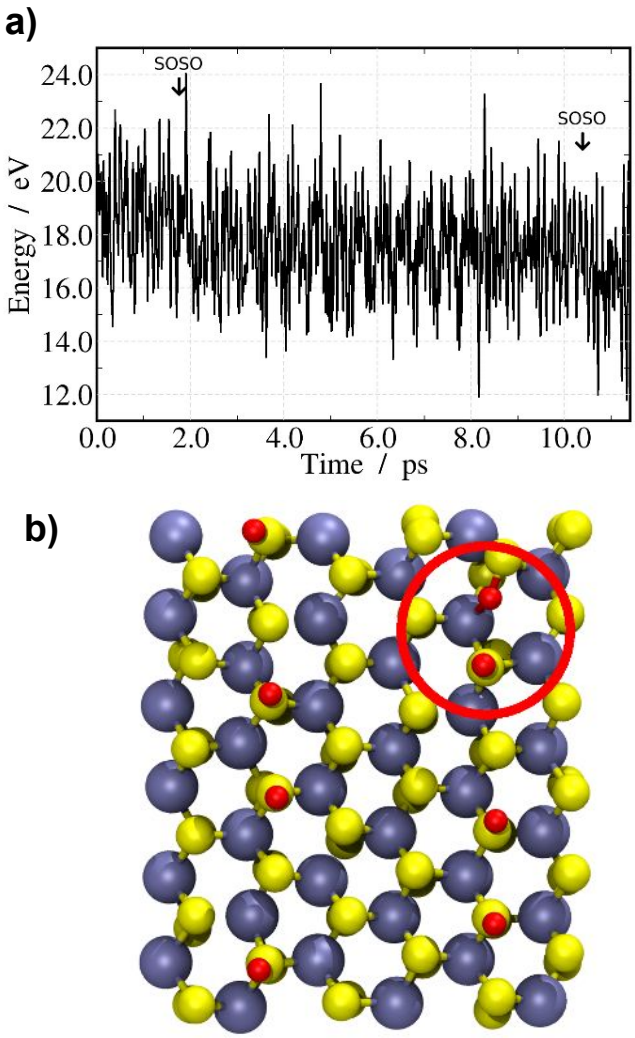

Figure 5. a) Total energy as a function of time for AIMD simulation of SO+SOMo intermediates showing the conversion to SO+SO intermediates. **b)** Snapshot of the cell structure at the end of the simulation, showing that only one SO+SOMo intermediate remained unreacted (red circle).

not lead to OSOMo due to the kinetics considerations outlined above. The fact that the direct desorption of SO was never observed from the SO+SO intermediate in the AIMD simulations is consistent with the large energy barrier of 3.13 eV for the desorption process as obtained from a NEB calculation (Figure S6).

As the OSOMo is the key intermediate leading to the release of SO and SO_2 species to the gas phase, we performed additional simulations at longer time to further verify the desorption mechanisms. Figure 6a shows the simulation cell with four OSOMo intermediates (previously thermalized at 1500 K for 1 ps). The desorption processes are indicated together with the energy profile in Figure 6b and relevant snapshots are shown in Figure 6c (side and top views, gas-phase molecules not shown in top views for clarity).

Direct SO_2 desorption from the OSOMo is observed at 1.835 ps and 2.406 ps (Figure 6c), leaving two S-vacancies on the surface. At 6.5 ps an OSOMo → Mo–OSO conversion process occurs and upon breakage of the O−S bond of Mo–OSO at 7.1 ps, a SO molecule is released into the gas phase leaving an oxygen atom on the surface (Figure 6c at 8.505 ps). The last OSOMo intermediate remaining produces the desorption of another SO_2 molecule at 10.503 ps. The snapshot at 11.078 ps in Figure 6c shows one SO and three SO_2 molecules in the gas phase. Finally, at around 12 ps there is a large decrease in the energy profile in Figure 6b. It is due to the adsorption of the SO molecule on an S-vacancy surface site (Figure 6c at 12.733 ps). This process is very exothermic with ΔE = -3.13 eV (Figure S6).

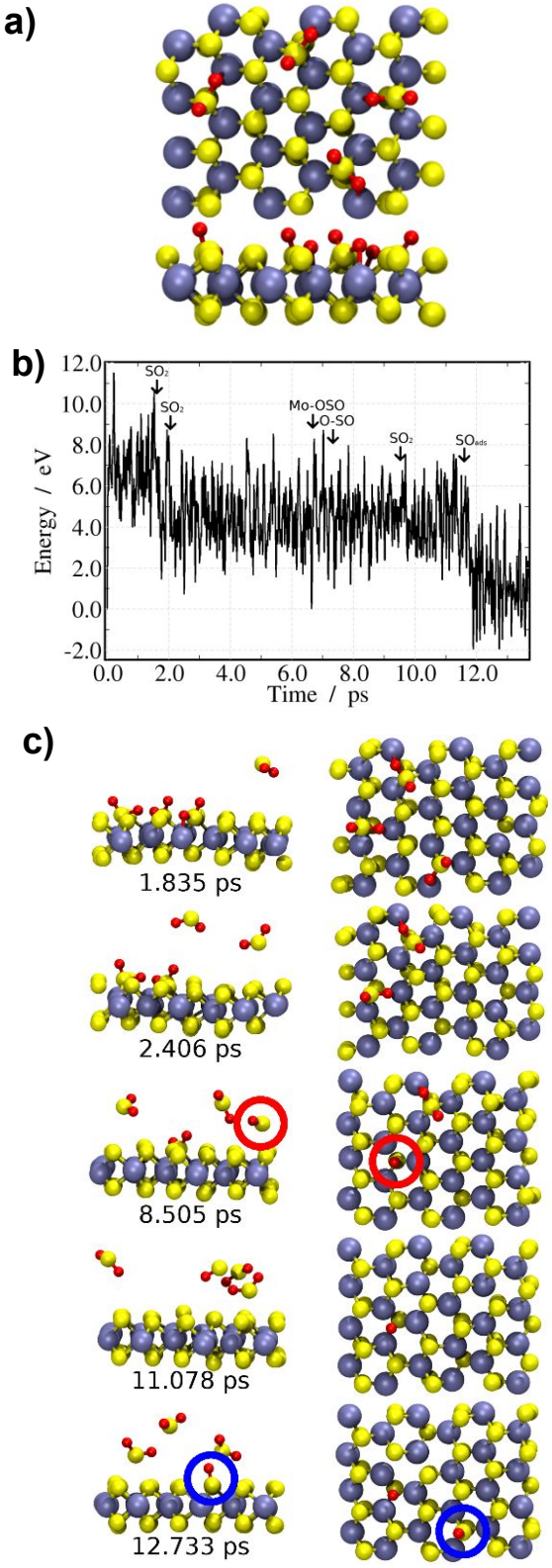

Figure 6. a) Top and side views of the simulation cell initially containing four OSOMo intermediates. **b)** Total energy vs time for AIMD simulation at 1500 K. The labels indicate the structural transformation taking place. **c)** Snapshots showing desorption of first SO_2 molecule (1.835 ps), second SO_2 molecule (2.406 ps), SO molecule (8.505 ps, red circle) and third SO_2 molecule (11.078 ps). *Adsorption* of SO on a sulfur vacancy site is observed at 12.733 ps (blue circle). Gas phase molecules not shown in top view.

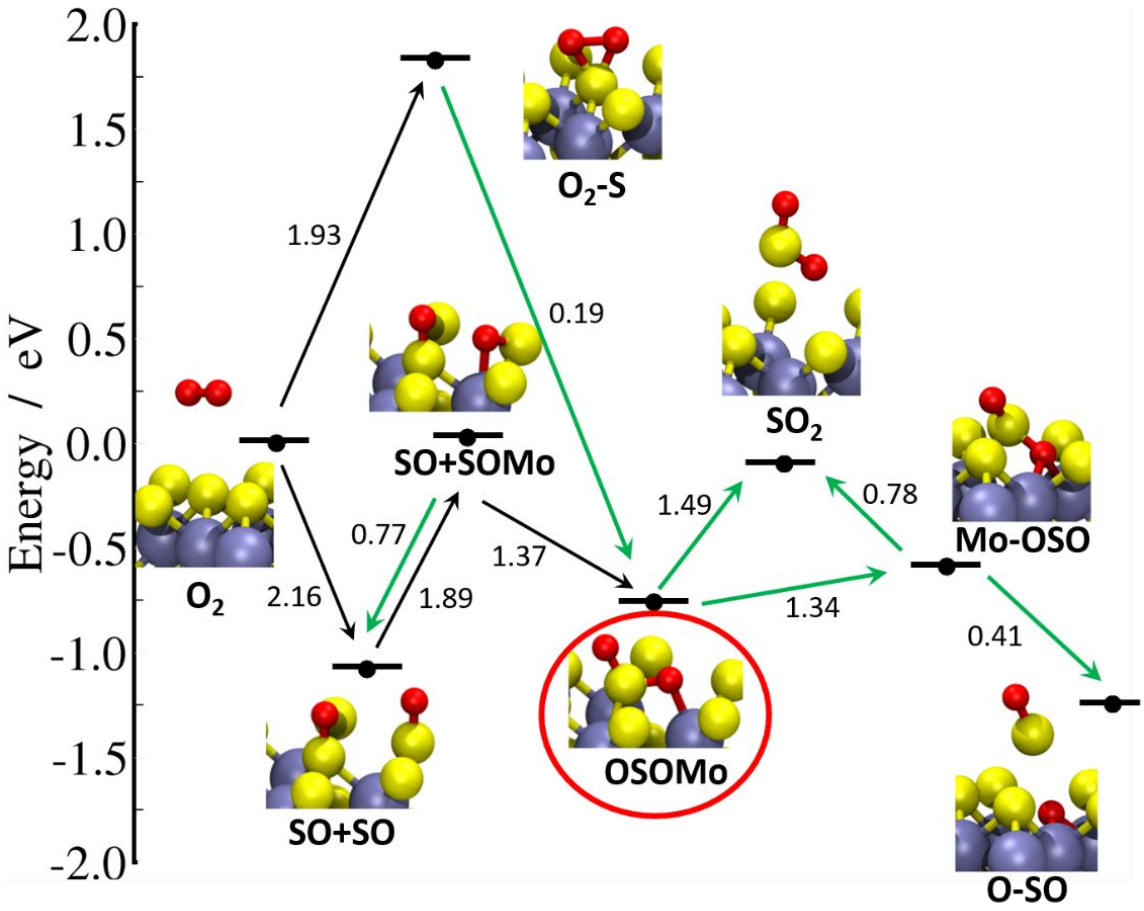

Figure 7. Summary of reaction mechanisms. Energy levels indicate the relative energy of each intermediate with respect to the reacting O_2 molecule adsorbed ontop of an S atom of MoS_2. The arrows correspond to elementary reaction steps and the number near each arrow is the activation energy barrier in eV. The green arrows correspond to processes that were observed in the AIMD simulations.

Figure 7 summarizes the most likely reaction mechanisms emerging from the calculations of the previous sections. The different species are located in the energy scale according to their relative energy with respect to the reactants (the O_2 molecule adsorbed ontop of an S atom of MoS_2). The number near the arrows indicates the activation energy barrier of a given elementary reaction step. The green arrows show the processes that were observed in the AIMD simulations. Figure 7 outlines the central role of the OSOMo intermediate. The reaction of O_2 with MoS_2 does lead to the OSOMo intermediate in a single elementary reaction step. It can be reached via the SO+SO or the O_2-S intermediates, with high energy barriers of 2.16 and 1.93 eV, respectively. The OSOMo intermediate can directly lead to the release of SO_2 (E_a=1.49 eV) or it may rearrange into the Mo-OSO intermediate (E_a=1.34 eV). From this intermediate both SO_2 (E_a=0.78 eV) and SO (E_a=0.41 eV) can be liberated, generating a sulfur vacancy in the first case and a substitutional O atom in the second case.

3.3 Top vs subsurface oxygen diffusion. The diffusion of O atoms is a competing process to those presented in Figure 2a. Therefore, we investigated the energetics of both the top and subsurface oxygen diffusion. The top diffusion of oxygen was never observed in the simulations, which is consistent with the high energy barrier of 2.38 eV shown in the NEB calculation of Figure 8a, which is in good agreement with the value of 2.53 eV reported in the literature.[33] A process with a lower energy barrier (1.92 eV, red curve in Figure 8a) is the formation of a SOMo moiety which occurs when the O atom of SO becomes a subsurface O atom by forming a bond with a Mo atom. Therefore, for an O atom bound on top of an S atom of MoS_2, it is more energetically favorable to insert into the surface giving rise to a a SOMo moiety, than to diffuse to an adjacent S atom forming a new SO moiety. Panels I-III in Figure 8b show the top diffusion process whereas panels I, IV, and V show the insertion of the O atom of SO into the surface to yield de SOMo moiety (panel V).

The O atom in the SOMo moiety may jump to an adjacent Mo atom while remaining bonded to the same S atom. The black curve in Figure 8c shows the corresponding energy profile and panels I-III in Figure 8d show the initial structure, an intermediate (O atom bound to both Mo atoms), and the final state. This process has an energy barrier of 1.80 eV. Another possibility is the jump of the O atom of the SOMo moiety to an adjacent S atom while remaining bonded to the same Mo atom. This process is shown in pannels I, IV, and V of Figure 8d, and the corresponding energy profile (red filled circles in Figure 8c), shows an energy barrier of 1.80 eV. When this oxygen jump occurs towards the S atom of an adjacent SO group (panels I', VI and VII in Figure 8d), the energy profile (red open symbols in Figure 8c) has a lower barrier (1.30 eV) and the reaction becomes exothermic (ΔE = -0.79 eV) as the stable OSOMo intermediate is formed (panel VII in Figure 8d) which, as discussed above, is the key intermediate leading to the desorption of both SO and SO_2 species.

Energy profiles comparing the top and subsurface diffusions of the oxygen atom are presented in Figure 8e. In the case of top O diffusion, the energy profile corresponds to two successive oxygen jumps (with E_a=2.38 eV) as indicated by the black arrows in the inset. The subsurface diffusion (red arrows) has a lower energy barrier and a more complex profile as it involves the oxygen jump between adjacent S atoms (while bonded to the same Mo atom, E_a=1.8 eV) and next the jump to an adjacent Mo atom (while bonded to the same S atom, E_a=0.83 eV), as shown by the red arrows in the inset of Figure 8e. As expected, the breakage of the covalent and directional O–S bonds has a much higher energy barrier than the breakage of the more ionic and delocalized O–Mo bonds.

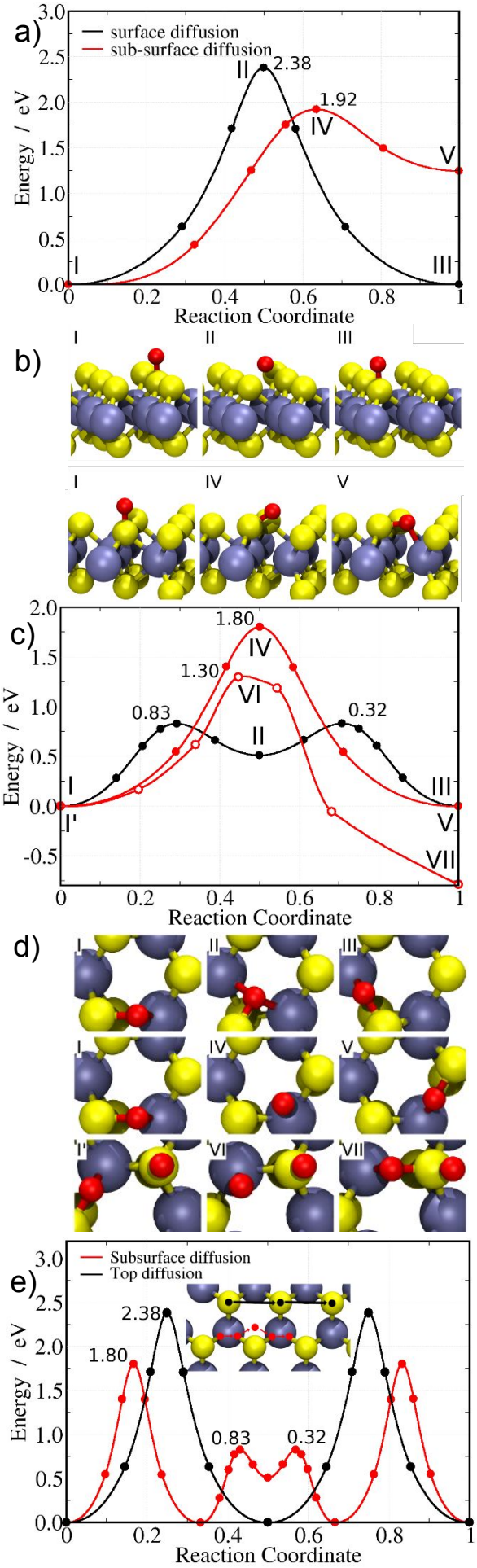

Figure 8. a) Energy profiles obtained from NEB calculations for surface (black curve) and sub-surface (red curve) diffusion. The numbers show energy barriers. **b)** Structure of reactants, transition state and products for surface (panels I-III) and subsurface diffusion (panels I', IV and V). **c)** Energy profiles for subsurface diffusion processes: O diffusion around an S atom (black curve), O diffusion towards adjacent S atom (red curve, filled circles) and O diffusion towards SO group (red curve, open circles). **d)** Panels showing oxygen diffusion along the different paths indicated in c). **e)** Summary of subsurface and top diffusion energy profiles along the surface sites indicated by the arrows in the inset. The numbers indicate energy barriers in eV with respect to the previous energy minimum.

4. Conclusions

The first steps in the oxidation of MoS_2 with O_2 occur along two branches in the reaction mechanism which are characterized by two stable intermediates. First, dissociative adsorption of O_2 may produce two adjacent SO groups in an exothermic reaction with ΔE = -1.08 eV with a large energy barrier of 2.16 eV. The direct desorption of SO leaving a sulfur vacancy on the surface is very costly with ΔE = 3.13 eV. Although the NEB calculations show that from an energetic point of view other intermediates may be reached in the path towards SO_2 desorption, the AIMDS simulation showed that this path is very unlikely and it was never observed even though high temperatures were employed.

In the second reaction branch, the OSOMo intermediate is formed with ΔE = -0.71 eV and an energy barrier of 1.93 eV. It consists of one SO group with an O atom inserted into one of the three Mo−S bonds (O=S−O−Mo moiety). The AIMD simulations, in agreement with the NEB energy profiles, show that SO_2 can directly desorb from this intermediate. In turn, the rearrangement of the OSOMo intermediate produces a new intermediate (Mo−OSO) from which both SO and SO_2 can desorb. The desorption of SO_2 leaves a sulfur vacancy, whereas the desorption of SO, leaves an O atom in replacement of the desorbed S atom. This reaction is the most exothermic with ΔE = -1.20 eV. Diffusion of oxygen atoms may also occur, with subsurface diffusion (involving O–S and O–Mo bonds) having lower energy barriers than O diffusion on top of surface S atoms (only O–S bond formation/breakage).

In summary, our combined NEB and AIMD investigation has provided insights into the energetics and dynamics of the initial stages of MoS_2 etching induced by O_2 as well as on the mechanisms leading to the formation of substitutional oxygen, which has been recently recognized as prolific point defect in transition metal dichalcogenides[13,34] which is responsible for the activation of the basal plane of MoS_2.[12,18,19,35]

Associated Content

The Supporting Information is available free of charge on the ACS Publications website. Additional NEB and AIMD simulations.

Author Information

Corresponding Author Email: mpatrito@gmail.com (E.M.P.)

Notes

The authors declare no competing financial interest.

Acknowledgments

EMP acknowledges funding from Foncyt (PICT-2014-2199) and Secyt-UNC. This work used computational resources from CCAD – Universidad Nacional de Córdoba (http://ccad.unc.edu.ar/), which is part of SNCAD – MinCyT, República Argentina.

References

(1) Lembke, D.; Bertolazzi, S.; Kis, A. Single-Layer MoS_2 Electronics. *Acc. Chem. Res.* **2015**, *48*, 100-110.

(2) Park, W.; Park, J.; Jang, J.; Lee, H.; Jeong, H.; Cho, K.; Hong, S.; Lee, T. Oxygen Environmental and Passivation Effects on Molybdenum Disulfide Field Effect Transistors. *Nanotechnology* **2013**, *24*, 09520.

(3) Gao, J.; Li, B.; Tan, J.; Chow, P.; Lu, T.-M.; Koratkar, N. Aging of Transition Metal Dichalcogenide Monolayers. *ACS Nano* **2016**, *10*, 2628-2635.

(4) Budania, P.; Baine, P.; Montgomery, J.; McGeough, C.; Cafolla, T.; Modreanu, M.; McNeill, D.; Mitchell, N.; Hughes, G.; Hurley, P. Long-Term Stability of Mechanically Exfoliated MoS_2 Flakes. *MRS Commun.* **2017**, *7*, 813-818.

(5) Lv, D.; Wang, H.; Zhu, D.; Lin, J.; Yin, G.; Lin, F.; Zhang, Z.; Jin, C. Atomic Process of Oxidative Etching in Monolayer Molybdenum Disulfide. *Sci. Bull.* **2017**, *62*, 846-851.

(6) Yamamoto, M.; Einstein, T. L.; Fuhrer, M. S.; Cullen, W. G. Anisotropic Etching of Atomically Thin MoS_2. *J. Phys. Chem. C* **2013**, *117*, 25643-25649.

(7) Wu, J.; Li, H.; Yin, Z.; Li, H.; Liu, J.; Cao, X.; Zhang, Q.; Zhang, H. Layer Thinning and Etching of Mechanically Exfoliated MoS_2 Nanosheets by Thermal Annealing in Air. *Small* **2013**, *9*, 3314-3319.

(8) Zhen, H.; Qin, X.; Cheng, L.; Azcatl, A.; Kim, J.; Wallace, R. M. Remote Plasma Oxidation and Atomic Layer Etching of MoS_2. *ACS Appl. Mater. Interfaces* **2016**, *8*, 19119-19126.

(9) Rao, R.; Islam, A. E.; Campbell, P. M.; Vogel, E. M.; Maruyama, B. In situ thermal oxidation kinetics in few layer MoS_2. *2D Mater.* **2017**, *4*, 025058.

(10) Walter, T. N.; Kwok, F.; Simchi, H.; Aldosari, H. M.; Mohney, S. E. Oxidation and Oxidative Vapor-Phase Etching of Few-Layer MoS_2. *J. Vac. Sci. Technol., B: Nanotechnol. Microelectron.: Mater., Process., Meas., Phenom.* **2017**, *35*, 021203.

(11) Spychalski, W. L.; Pisarek, M.; Szoszkiewicz, R. Microscale Insight into Oxidation of Single MoS_2 Crystals in Air. *J. Phys. Chem. C* **2017**, *121*, 26027-26033.

(12) Pető, J.; Ollár, T.; Vancsó, P.; Popov, Z. I.; Magda, G. Z.; Dobrik, G.; Chanyong, H.; Sorokin, P. B.; Tapasztó, L. Spontaneous Doping of the Basal Plane of MoS_2 Single Layers Through Oxygen Substitution under Ambient Conditions. *Nat. Chem.* **2018**, *10*, 1246-1251.

(13) Grønborg, S. S.; Thorarinsdottir, K; Kyhl, L.; Rodriguez-Fernández, J; Sanders, C. E.; Bianchi, M.; Hofmann, P.; Miwa, J. A.; Ulstrup, S.; Lauritsen, J. V. Basal Plane Oxygen Exchange of Epitaxial MoS_2 without Edge Oxidation. *2D Mater.* **2019**, *6*, 045013.

(14) Jia, F.; Liu, C.; Yang, B.; Song, S. Microscale Control of Edge Defect and Oxidation on Molybdenum Disulfide through Thermal Treatment in Air and Nitrogen Atmospheres. *Appl. Surf. Sci.* **2018**, *462*, 471- 479.

(15) Ugonna Ukegbu, U.; Szoszkiewicz, R. Microscopic Kinetics of Heat-Induced Oxidative Etching of Thick MoS_2 Crystals. *J. Phys. Chem. C* **2019**, *123*, 22123-22129.

(16) Maguire, P.; Jadwiszczak, J.; O'Brien, M.; Keane, D.; Duesberg, G. S; McEvoy, N.; Zhang, H. Defect-moderated Oxidative Etching of MoS_2. *J. Appl. Phys.* **2019**, *126*, 164301.

(17) Kibsgaard, J.; Chen, Z.; Reinecke, B. N.; Jaramillo, T. F. Engineering the Surface Structure of MoS_2 to Preferentially Expose Active Edge Sites for Electrocatalysis. *Nat. Mater.* **2012**, *11*, 963–969

(18) Xie, J.; Zhang, J.; Li, S.; Grote, F.; Zhang, X.; Zhang, H.; Wang, R.; Lei, Y.; Pan, B.; Xie, Y. Controllable Disorder Engineering in Oxygen-Incorporated MoS_2 Ultrathin Nanosheets for Efficient Hydrogen Evolution. *J. Am. Chem. Soc.* **2013**, *135*, 17881-17888.

(19) Zhou, J.; Fang, G. Z.; Pan, A. Q.; Liang, S. Q. Oxygen-Incorporated MoS_2 Nanosheets with Expanded Interlayers for Hydrogen Evolution Reaction and Pseudocapacitor Applications. *ACS Appl. Mater. Interfaces* **2016**, *8*, 33681-33689.

(20) Walter, T. N.; Kwok, F.; Simchi, H.; Aldosari, H. M.; Mohney, S. E. Oxidation and Oxidative Vapor-Phase Etching of Few-Layer MoS_2. *J. Vac. Sci. Technol., B: Nanotechnol. Microelectron.: Mater., Process., Meas., Phenom.* **2017**, *35*, 021203.

(21) Martincová, J.; Otyepka, M.; Lazar, P. Is Single Layer Mos_2 Stable in the Air? *Chem. - Eur. J.* **2017**, *23*, 13233-13239.

(22) Tagawa, M.; Yokota, K.; Ohmae, N.; Matsumoto, K.; Suzuki, M. Hyperthermal Atomic Oxygen Interaction with MoS_2 Lubricants Relevance to Space Environmental Effects in Low Earth Orbit - Atomic Oxygen-Induced Oxidation. *Tribol. Lett.* **2004**, *17*, 859-865.

(23) Santosh, K. C., Longo, R. C., Wallace, R. M. & Cho, K. Surface Oxidation Energetics and Kinetics on MoS_2 Monolayer. *J. Appl. Phys.* **2015**, *117*, 135301

(24) Longo, R. C.; Addou, R.; Santoch, K. C.; Noh, J.-Y.; Smyth, C. M.; Barrera, D.; Zhang, C.; Hsu, J. W. P.; Wallace, R. M.; Cho, K. Intrinsic Air Stability Mechanisms of Two Dimensional Transition Metal Dichalcogenide Surfaces: Basal versus Edge Oxidation. *2D Materials*, **2017**, *4*, 025050.

(25) Perdew, J. P.; Burke, K.; Ernzerhof, M. Generalized Gradient Approximation Made Simple. *Phys. Rev. Lett.* **1996,** *77*, 3865-3868.

(26) Vanderbilt, D. Soft self-consistent Pseudopotentials in a Generalized Eigenvalue Formalism. *Phys. Rev. B* **1990,** *41*, 7892-7895.

(27) Giannozzi, P.; Baroni, S.; Bonini, N.; Calandra, M.; Car, R.; Cavazzoni, C.; Ceresoli, D.; Chiarotti, G. L.; Cococcioni, M.; Dabo, I. et al. QUANTUM ESPRESSO: a Modular and open-Source Software Project for Quantum Simulations of Materials. *J. Phys. Cond. Matt.* **2009,** *21*, 395502.

(28) Grimme, S. Semiempirical GGA-type Density Functional Constructed with a Long-Range Dispersion Correction. *J. Comput. Chem.* **2006**, *27*, 1787-1799.

(29) Barone, V.; Casarin, M.; Forrer, D.; Pavone, M.; Sambi, M.; Vittadini, A. Role and Effective Treatment of Dispersive Forces in Materials: Polyethylene and Graphite Crystals as Test Cases. *J. Comput. Chem.* **2009**, *30*, 934-939.

(30) Henkelman, G.; Uberuaga, B. P.; Jónsson, H. A Climbing Image Nudged Elastic Band Method for Finding Saddle Points and Minimum Energy Paths. *J. Chem. Phys.* **2000,** *113*, 9901-9904.

(31) Monkhorst, H. J.; Pack, J. D., Special Points for Brillouin-Zone Integrations. *Phys. Rev. B* **1976,** *13*, 5188-5192.

(32) Karlický, F.; Lazar, P.; Dubecký, M.; Otyepka, M. Random Phase Approximation in Surface Chemistry: Water Splitting on Iron. *J. Chem. Theory Comput.* **2013**, *9*, 3670−3676.

(33) Liu, H.; Han, N.; J. Zhao. Atomistic Insight into the Oxidation of Monolayer Transition Metal Dichalcogenides: from Structures to Electronic Properties. *RSC Adv.* **2015**, *5*, 17572-17581.

(34) Barja, S.; Refaely-Abramson, S.; Schuler, B.; Qiu, D. Y.; Pulkin, A.; Wickenburg, S.; Ryu, H.; Ugeda, M. M.; Kastl, C.; Chen, C. Identifying Substitutional Oxygen as a Prolific Point Defect in Monolayer Transition Metal Dichalcogenides. *Nat. Commun.* **2019**, *10*, 3382.

(35) Li, G.; Zhang, D.; Qiao, Q.; Yu, Y.; Peterson, D.; Zafar, A.; Kumar, R.; Curtarolo, S.; Hunte, F.; Shannon, S.; Zhu, Y.; Yang, W.; Cao, L. All the Catalytic Active Sites of MoS_2 for Hydrogen Evolution. *J. Am. Chem. Soc*. **2016,** *138*, 16632-16638.

TOC Graphic